INTERNATIONAL JOURNAL OF PLANT, ANIMAL AND ENVIRONMENTAL SCIENCES
IJPAES

Volume-6, Issue-1, Jan-Mar-2016 Coden: IJPAJX-CAS-USA, Copyrights@2016 ISSN-2231-4490

Received: 4th Jan-2016 Revised: 18th Jan 2016 Accepted: 20th Jan 2016

Research article

EFFICIENT VISIBLE LIGHT ACTIVE NANOSTRUCTURED TIO_2 (CORE)-POLYANILINE (SHELL) PHOTOCATALYST FOR SIMULTANEOUSLY REMOVING OF COOKING OIL FUMES

Bao Lin and Shu-Liang Liaw

Graduate Institute of Environmental Engineering, National Central University 300 Jhongda Road, Jhongli, Taoyuan, Taiwan

ABSTRACT: Cooking oil fumes (COFs) deteriorate indoor air quality. Therefore, in this study, a nanostructured TiO_2 core–porous polyaniline shell (TP) nanocomposite was developed for vapor-phase photocatalytic degradation of volatile organic compounds (VOCs) from COFs. A PANI shell coated uniformly on the surface of the TiO_2 core was prepared through a double–surfactant-assisted polymerization method. The PANI shell thickness, morphology characterizations and specific surface area were controlled by altering the weight ratio of aniline monomer to TiO_2 (AT ratio). Under the illumination of ultraviolet-visible light, the TP nanocomposite exhibited higher photocatalytic activity than did pure TiO_2 because of the charge-separation and charge-transfer processes from TiO_2 to PANI shell as well as the high specific surface area induced by the reduced aggregation states of the TiO_2 nanoparticles. Under the characteristic AT ratio of 2.5, The TP nanocomposite containing the nanoporous PANI shell that was coated on the TiO_2 nanoparticle core continuously treated the COFs, demonstrating a VOC removal efficiency of approximately 80% and mineralization efficiency of approximately 46 %; the thermal tolerance was as high as 125°C.

Key words: cooking oil fumes, indoor air, VOCs, photocatalytic oxidation, polyaniline, TiO_2

*Corresponding author: Bao Lin, Graduate Institute of Environmental Engineering, National Central University 300 Jhongda Road, Jhongli, Taoyuan, Taiwan Email: a88880839@yahoo.com.tw Tel: +886-2772-0922; Fax: +886-2550-8047

INTRODUCTION

The emission of volatile organic compounds (VOCs) from cooking oil fumes (COFs) is a serious problem because of its mutagenicity and carcinogenicity [1]. Reported technologies for VOCs removal include biofilters, wet scrubbers, catalytic oxidation and iron-based catalytic ozonation [2–6]. However, these technologies cannot be used because of their large size, high capital and maintenance costs, and the formation of undesirable byproducts that require additional treatments.

Ultraviolet (UV)/TiO_2 technology is widely studied for the photocatalytic degradation of pollutants in indoor air. However, the photocatalytic activity of this technology is limited because the wide band gap of TiO_2 (3.2 eV) enables it to absorb only UV light (< 387 nm) constituting only a small fraction (3%–5%) of solar photons [7]. Surface dye sensitization of TiO_2 has been extensively applied for improving the photocatalytic activity of TiO_2 [8–10]; however, this technique is marred by the dissolution and photocatalytic degradation of dyes.

Conducting polymers with extended π–conjugated electron systems have been extensively studied because of their remarkable low-energy optical transitions and low ionization potential. Accordingly, such polymers can act as photosensitizers to sensitize TiO_2 through the absorption of a broad spectrum of UV and visible light (190–800 nm) irradiations [11–13]. Among the conducting polymers, polyaniline (PANI) has attracted considerable interest because of its high stability, low cost, and ease of synthesis [14–16]. Therefore, in this study, we developed a core–shell nanostructured TiO_2–porous PANI (TP) nanocomposite for the simultaneous removal of VOCs from COFs.

In situ polymerization of aniline in the presence of TiO_2 nanoparticles has been frequently used for preparing core–shell PANI–TiO_2 nanocomposite [17–19]. Because nano–sized TiO_2 nanoparticles in aqueous solution are easily agglomerated (Borodko et al., 2006) [20], this agglomeration deteriorates the photocatalytic activity of such nanoparticles by reducing their effective surface area. In addition, in situ polymerization is executed under an extremely acidic condition, and this may generally result in TiO_2 nanoparticle cores being etched away during polymerization processes.

In this work, we applied a double–surfactant support polymerization method and to control the polymerization of PANI onto the surface of TiO_2 [21, 22]. The PANI thickness, morphology characterizations and light adsorption were studied as a function of the weight ratio of aniline monomer to TiO_2 (AT ratio). After optimizing the AT ratio, the adsorption and oxidation of COFs by photocatalytic oxidation at the TiO_2 (core)–PANI (shell) nanocomposite (TP nanocomposite) surface were performed. Gas-phase characterization enabled examining the surface oxidation mechanisms. In addition, thermal stability is important for the catalyst because an unpredictable amount of steam is produced during cooking, high thermal energy causes any moisture coated on the surface of the catalyst pellets to evaporate, thus increasing the gas–solid mass transfer coefficients. A long-term test was continuously conducted to treat COFs for 300 h to evaluate the thermal durability.

EXPERIMENTAL AND METHODS

Preparation of the TiO2 Core

TiO2 nanoparticles (mean crystallite size = 50 μm; mean pore size = 20 nm) served as the catalyst core. The selected TiO_2 nanoparticles (100 g) were dispersed in deionized water (1000 mL), and polyethylene glycol (PEG; 150 g) was added to this dispersion and then constantly stirred for 24 h. After the stirring was completed, the nanoparticles were washed repeatedly with dilute acetone until the unabsorbed PEG molecules were completely removed. Subsequently, the PEG–absorbed TiO_2 nanoparticles were dried at 60°C for another 24 h.

Synthesis of the Core–Shell Nanocomposites

The required amount of aniline monomer (Merck Company, Germany) was distilled for 60 min under vacuum and stored at 5°C before use. The PEG-absorbed TiO_2 nanoparticles (100 g), dodecyl benzene sulfonic acid (DBSA;20 g), potassium persulfate (20g) and1000 mL pure water were thoroughly mixed using to obtain a uniform suspension. The aniline monomer and 500 mL of HCl solution (20 mM) were subsequently added to the derived suspension. The mixture was slowly stirred at room temperature for 24 h for polymerization. After the polymerization process was completed, the sample solution in the sample holder was cooled and completely frozen at -40°C. The obtained frozen samples were subsequently freeze-dried for 48 h in a vacuum chamber. Throughout the experiments, the AT ratios were varied from 0.5 to 3.5 at intervals of 0.5. To measure the PANI shell thickness, the resulting TP products were immersed in 1.0 M HCl for 24 h. Hollow PANI capsules were obtained from the TP products by using 1 wt % HF to etch the silica layer and 1.0 M HCl to etch the TiO_2 core [23]. Furthermore, the obtained TP sample was coated on 200 g of a honeycomb ceramic substrate under vacuum. The coating steps followed those described in the U.S. patent 7,521,087 (Bull et al., 2009) [24].

COF testing

The experimental setup mainly linked the catalytic reactor to a 2-L impinger, which was filled with 1 L of sunflower cooking oil of Taiwan origin (Figure 1). The oil was heated to its smoke point (180 °C) to produce COFs [25]. The batch-scale adsorption and oxidation procedure consisted of five major steps: (i) activating the catalyst sample at 150 °C for 1 h to remove water and other adsorbed hydrocarbon species to guarantee surface repeatability; (ii) adsorbing COFs on the catalyst surface (the COFs passes through the sorbent sites until they are saturated); (iii) flushing the adsorbent bed with dry air flow to remove reversibly adsorbed species and desorb the molecules with the weakest heat of adsorption (i.e., physisorbed species, leaving only the irreversibly adsorbed molecules on the catalyst surface); (iv) achieving surface exposition by switching on visible (150 W tungsten-halogen lamp) and UV illumination (150 W); (v) closing the visible and UV illumination after 60 min and purging the system under a dry synthetic air flow for 30 min.

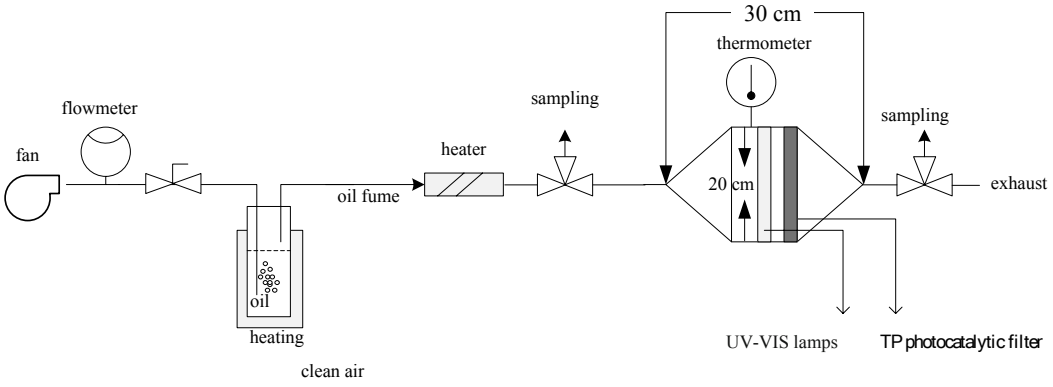

Fig-1: Experimental setup for the COFs test.

After the aforementioned test was completed, the COFs was continuously introduced to the catalytic filter. The operational conditions used in the experiment are listed in Table 1. The COFs was sampled on-line before and after the treatment for composition characterization.

Table 1 Experimental condition in the COFs testing

Condition	Value
Gas flow rate (L/min)	10
Reaction temperature (°C)	25–300
Relative humidity (%)	0
Retention time (s)	0.5
Initial THC concentration of COF (ppm)	100–120
Duration of adsorption and oxidation test (h)	2
Duration of long-term test in each run (h)	300

Analyses

The morphology of the samples was observed under a Cam Scan MV 2300 scanning electron microscope (SEM) with an accelerating voltage of100 kV. X-ray diffraction (XRD) patterns were taken on a Siemens D5000 X-ray diffractometer with a Cu Kα X-ray radiation (λ= 0.154 nm). Specific surface area measurements of the fresh catalyst were based on the N_2 adsorption–desorption porosimetry at 77 K, and the special surface areas were measured using the Brunauer–Emmett–Teller (BET) method (Micromeritics Gemini-2380). The mean pore diameter (in nm) was determined using the following equation [26]:

$$\bar{d} = (2 \times 10^{-3} e) / (S_{BET}) \quad (1)$$

where the pore volume (e) is expressed in cm^3/g and the BET surface area (S_{BET}) is expressed in m^2/g. A Shimadzu UV-1700 Farma spectrophotometer was used to record the UV-Vis-near IR spectra of catalysts.

The compounds of COFs were characterized using gas chromatography–mass spectroscopy (GC-MS, QP2010NC, Japan). The amount of CO_2 produced was determined using GC with a thermal conductivity detector (China Chromatography 3000, Taiwan). The photocatalytic activity of the TP sample was evaluated by the mineralization efficiency from the COFs to CO_2 as

$$\text{Mineralization efficiency (\%)} = (Q_{CO2}/Q_{COFs(irr)}) \times 100\% \quad (2)$$

where Q_{CO2} is the total amount of CO_2 resulting from the oxidation of COF, and $Q_{COFs(irr)}$ is the total quantity of COFs pollutants irreversibly adsorbed on the catalyst surface.

Total hydrocarbon (THC) concentrations were determined using gas chromatography with a flame ionization detector (China GC-8601, Taiwan). The removal efficiency of VOCs is calculated as follows:

$$Re = (C_{in} - C_{out})/C_{in} \times 100\% \quad (3)$$

where Re represents the removal efficiency, and C_{in} and C_{out} are the THC concentrations of VOCs before and after the catalytic reaction, respectively.

DISCUSSIONS

Physical properties of the TP samples

Figure 2 shows the XRD patterns of the TP samples obtained by altering the AT ratio. The patterns corresponded to pure TiO_2, and this finding is confirmed by JCPDS Pattern No. 21-1272 (anatase TiO_2) [27, 28]. The diffraction peaks of TiO_2 were adequately maintained in the TP samples, and the peak intensity of TiO_2 decreased as the content of PANI increased in the TP sample. The performance indicates that the crystallite size of TiO_2 remained unchanged during the polymerization process. Abroad diffraction peak centered at $2\theta = 25°$was observed for PANI, and this peak was overwhelmed by the strong diffraction peaks of TiO_2 in the TP materials. This indicates that the PANI layer had formed on the surface of the TiO_2 nanoparticles.

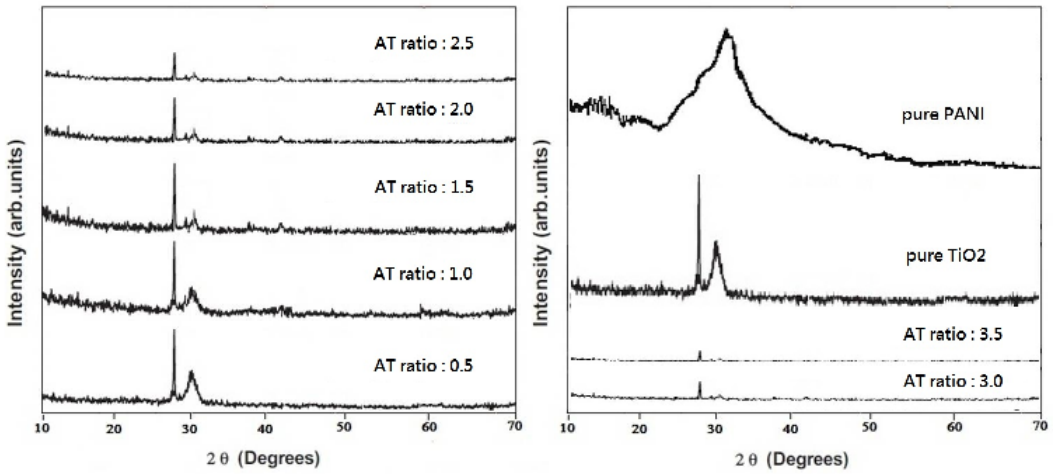

Fig-2: The XRD patterns with the AT ratio

The SEM results further confirm the successful polymerization of aniline onto the TiO_2 core (Figure 3a). The PANI particles and aggregation in the TP samples could not be found in the SEM images. The observation indicated that PANI was uniformly coated on the TiO_2 nanoparticles during the polymerization process. Figures 3(b) show the thicknesses of the PANI shell as a function of the various AT ratios. The shell thickness linearly increased with increasing AT ratio. These results mean that the experimental conditions can appropriately control the fabrication of the PANI shell on the surface of the TiO_2 core.

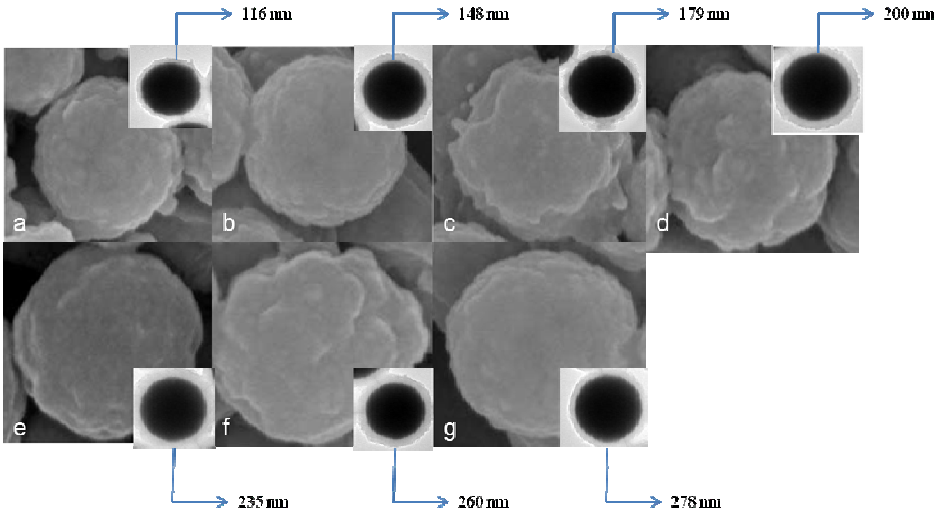

(a)

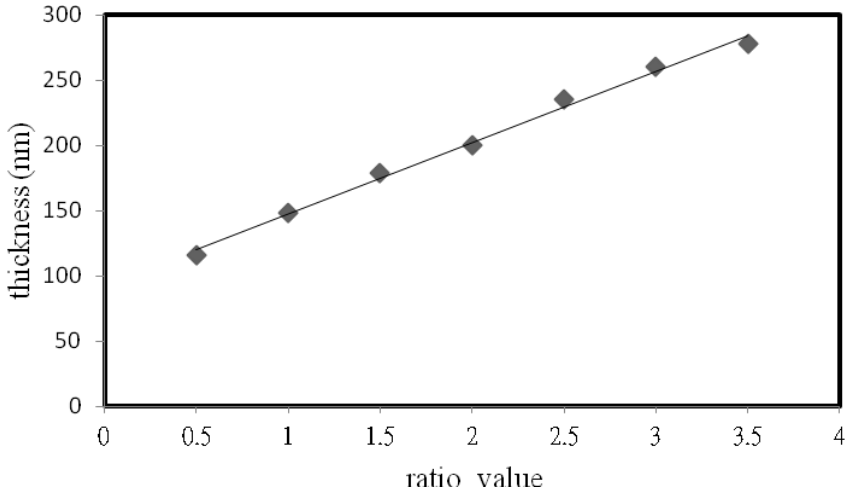

(b)

Fig-3: SEM images and thicknesses associated with the various AT ratio.

The forming mechanism of the PANI shell uniformly coated on the TiO_2 core is proposed as follows. In the double–surfactant polymerization, PEG and DBSA act as surfactants. Adding PVP can improve the dispersibility of the TiO_2 nanoparticles in aqueous solution. Before the polymerization reaction, DBSA was added to the PEG-absorbed TiO_2 solution. DBSA could dissociate into dodecyl benzene sulfonic (DBS) ions and a double-surfactant layer (PEG–DBS layer), which was expected to form with polar amide groups of PEG surrounded on the surface of the TiO_2 core and the negative side of DBS molecule facing out to the solution. Subsequently, aniline monomers were added and converted into cationic anilinium ions under an acidic condition.

The cationic anilinium ions were adsorbed on the surface of the negatively charged TiO_2 core because of electrostatic forces. The adsorption engendered a considerable increase in the local concentration of aniline monomers near the core surface. This consequently initiated the polymerization of aniline at low concentration of aniline monomers. Therefore, the polymerization was initiated, propagated, and terminated on the surface of the TiO_2 core rather than in solution. A homogeneous, continuous, and uniform PANI shell was eventually formed on the surface of the TiO_2 core.

According to the experimental data presented in Table 2, the TP nanocomposite with a AT ratio of 0.5 exhibited a specific surface area (S_{BET}) of 1430 m^2/g, mean pore size of 33.4 nm, and porosity of 75.4%. This S_{BET} value is evidently higher than a previously reported value [29], which can be attributed to the reduced aggregation states of the TiO_2 nanoparticles and the highly porous structure induced by the freeze-drying process in the synthesis of the core–shell nanocomposites [30]. In addition, the data of the materials slowly increased until the AT ratio reached 2.5, and subsequently, the data decreased as the AT ratio increased to 3. The performance can be explained by the pore formation of a freeze-dried polymer. Studies have reported that the freeze-drying technique is based on sublimation [31, 32]. The material to be dried is frozen quickly at a low temperature and then dried in a vacuum. The solvent molecules directly sublimate and escape as vapors, and porous structures are formed from the voids created by the removal of the solvent. Finally, a polymer porous film with an interpenetrating network structure can be obtained. When the PANI content is excessively low, the PANI shell structure demonstrates larger pores, preventing it from forming a stable porous surface. By contrast, when the PANI content is excessively high, maintaining satisfactory fluidity is difficult, affecting the growth of solvent crystals. The theory was confirmed with the SEM results. When the AT ratio was 0.5, the PANI shell demonstrated a nonuniform mesh-like structure (Figure 4a); when the ratio was 1–2, the shell exhibited a lamellar structure (Figures 4b–4d). Moreover, when the ratio was 2.5, the PANI shell demonstrated a lamellar structure, with nonuniform pores occurring between the polymer layers (Figure 4e). In addition, when the ratio was 3–3.5, the PANI shell exhibited lamellar polymer layers arranged in various orientations (Figures 4f–4g).

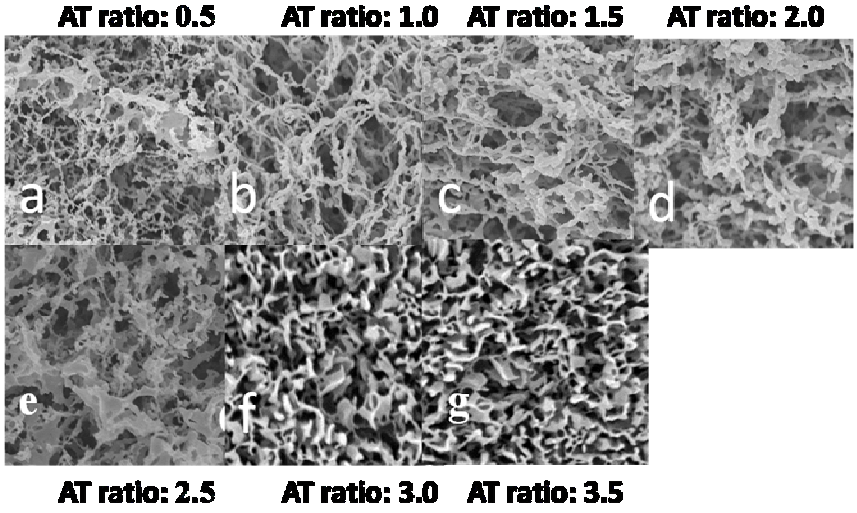

Fig-4: Surface structure characteristics associated with various AT ratio

Table 2: Physical characteristics associated with various AT ratio

Ratio value	S_{BET} (m^2/g)	Mean Pore size (nm)	Porosity (%)
0	147	20	34.52
0.5	1430	33.4	75.4
1.0	1431	42.5	78.6
1.5	1436	56.8	83.1
2.0	1442	76.8	86.5
2.5	1452	88.9	87.4
3.0	554	35.5	65.4
3.5	213	25.0	53.2

Light Absorption Characteristics of the TP Samples

Figure 5 displays the UV-visible Diffuse Reflectance Spectroscopy (DRS) spectra of pure TiO_2 and the TP nanocomposite with a AT ratio of 0.5. The DRS spectra of the TP nanocomposite with AT ratios of 1.0–3.5 are not included in the graph because they were similar to that of the nanocomposite with a AT ratio of 0.5. Pure TiO_2 exhibited only absorption lower than 390 nm, and the TP catalyst with the weight ratio of 0.5 demonstrated absorption peaks at 370 and 480 nm. The peak at 370 nm is attributed to the TiO_2 core in the TP nanocomposite, and that the broad absorption peaks at 480 nm are attributed to the $\pi \rightarrow \pi^*$ transition in the polymer chains [33]. Further, the observed tail indicating gradually increasing absorption into infrared region indicates charge carrier delocalization ($\tilde{n}\square^*$). The different light absorption characteristics correspond to weight ratios ranging from 1.0 to 3.5. These results indicate that PANI significantly increases the photoactive region of TiO_2 nanoparticles through the absorption of visible and near-IR radiation.

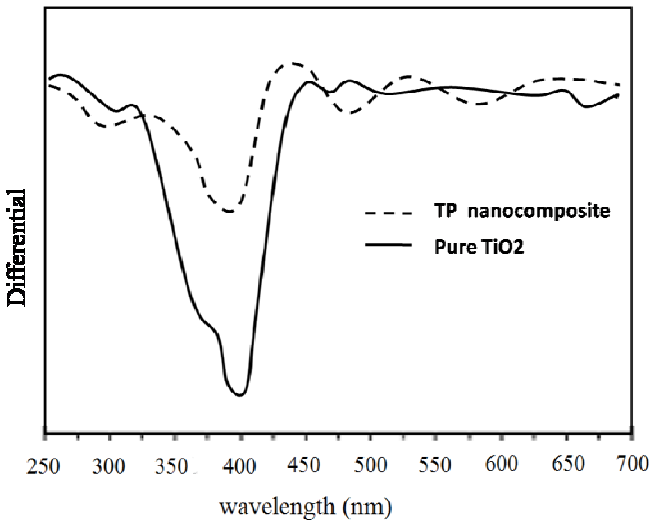

Fig-5: UV-VIS-NIR spectra of TP nanocomposite and pure TiO_2.

Adsorption and Oxidation of COFs through Photocatalytic Degradation

COFs containing a mean initial THC concentration of 110 ppm was introduced into the experimental apparatus at a flow rate of 1.0 L/min for 30 min (breakthrough). After 30 min, dry air was flushed into the apparatus. The COFs breakthrough and flushing curves for pure TiO_2 and the TP nanocmposite with characteristic AT ratio of 2.5 are shown in Figure 6.

The rising part of the curve corresponds to the adsorption of COFs on the catalyst. The decaying part of the curve corresponds to the desorption of the weakly bonded COFs from the catalyst surface. The difference between the flushing curve and the breakthrough curve enables determining the reversibly adsorbed fraction of COFs on the catalyst; that is, weakly bonded species. The amount of COFs irreversibly adsorbed on the surface of pure TiO_2 and the TP nanocomposite were 0.132 and 0.452 μg THC/m^2, respectively. This is obvious that higher specific surface area of the TP nanocomposite exhibited higher adsorption capacity than pure TiO_2.

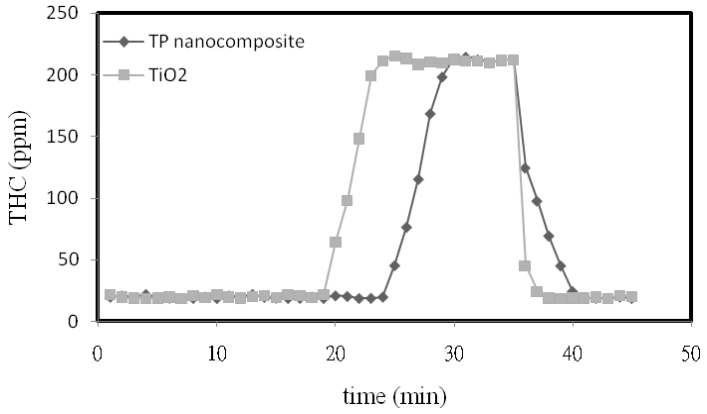

Fig-6: COFs breakthrough curve and flushing curve monitored on the surface of TP nanocomposite and pure TiO_2.

Following flushing, the surfaces of the photocatalyst samples were covered only by irreversibly adsorbed COFs. Figure 7 displays the evolution of CO_2 production during the exposure of COFs–irreversibly adsorbed catalyst surfaces to photocatalytic degrdation for 1 h until no more CO_2 products were detectable in exhaust. The amount of CO_2 produced for each catalyst was obtained through the integration of the respective temporal profiles listed in Table 3. From the data presented in Table 3 shows that TP composite has a CO_2 production (0.21 μg/m^2) and mineralization efficiency (45.13 %), which are obviously higher than those of pure TiO_2.

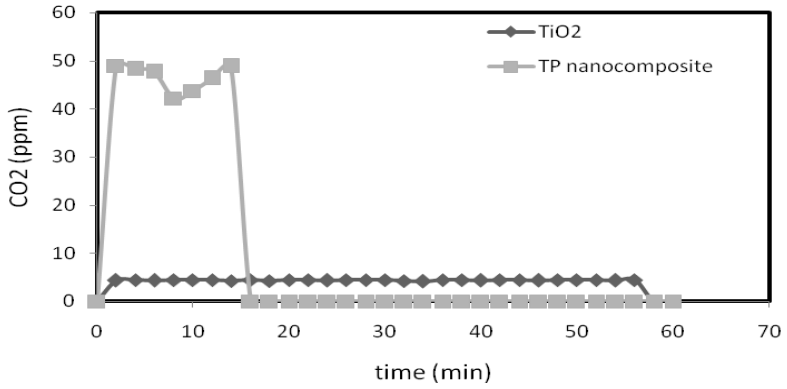

Fig-7: Mineralization performance after photocatalytic degradation

Table-3: The mineralization performance of COFs under photocatalytic oxidation of TP nanocomposite and pure TiO_2.

Photocatalyst	TiO_2	TP nanocomposite
CO_2 production (μg/m^2)	0.03	0.21
Mineralization efficiency (%)	3.66	45.13

The results reveal that the PANI content and high surface area were effective in enhancing the photoactivity. This study determined that the conduction position of TiO_2 was lower than the lowest unoccupied molecular orbital (LUMO) of PANI. The conduction band (CB) of TiO_2 can act as a sink for photogenerated electrons in the hybrid photocatalyst. When the PANI shell adsorbed visible light, the electrons were excited; the photoexcited electrons were injected into the CB of TiO_2, and the electrons in the TiO_2 valence band were delivered to the PANI shell [34]. Subsequently, the charge-separation and charge-transfer processes yielded OH radicals and superoxide radicals that could oxidize the adsorbent. In addition, the double–surfactant-assisted polymerization process reduced the aggregation states of the TiO_2 nanoparticles, and the freeze-drying process produced a highly porous PANI shell structure. These engendered a higher surface area and higher interaction between the TP nanocomposite and adsorbed VOCs compared with those associated with the pure TiO_2 nanoparticles [35].

In additional, it is reported that the pathway of the oxidation caused by the OH radicals attacks can be altered with the amount of OH radical [5]. When the VOCs are irreversibly adsorbed on the surface of photocatalyst, after the photodegradation, thus an insufficient amount of OH radicals degraded the VOCs into the complex intermediate products by an electron-transfer reaction. However, a sufficient amount of OH radicals directly mineralizes COFs to CO_2 and H_2O without the creation of additional intermediate products. This theory can be confirmed by the GC-MS results of photocatalytic treated COFs (Figure 8). The sunflower oil was mainly composed of saturated and unsaturated fats. Untreated COFs consisted mainly of alkenes, ketones, aldehydes, alcohols, and carboxylic acids. After the TiO_2 catalyst was passed, a considerable amount of intermediate products was generated. However, after the TP catalyst was passed, the number of components was significantly reduced, and no additional intermediate products were generated.

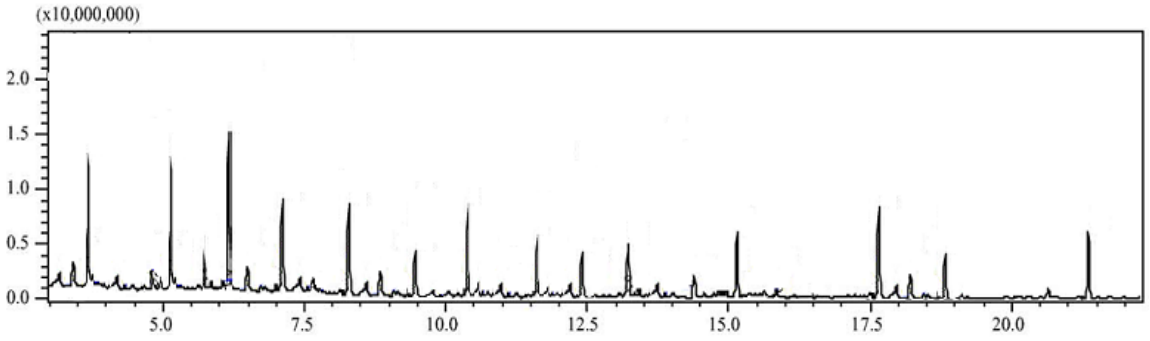

(a) untreated COFs

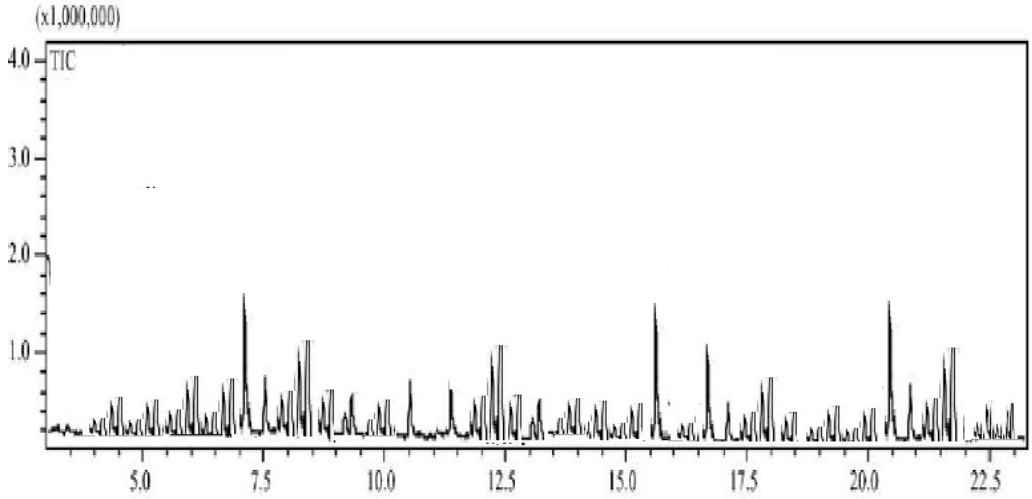

(b) TiO_2 catalytically treated COFs

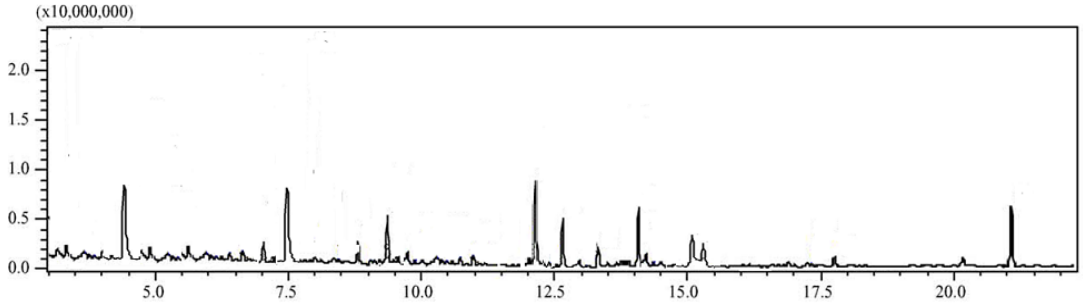

(c) TP nanocomposite catalytically treated COFs

Fig-8: GC–MS results of catalytically treated COFs.

Table-4: Chemicals in fume samples taken during experiments

Untreated COFs	2-Heptanone ketone, 4-pentenal, 2,2-dimethyl, ethanol, 2-butoxy-, ethanedioic acid, bis(1-methylpropyl) ester,2-heptenal, (Z)-,1-heptanol,1-octen-3-ol, 3-octanone, 2-pentyl-,3,7-decadiene, 2,9-dimethyl-,cyclohexanol, 2,4-dimethyl-, octanal, 4-ethylcyclohexanol,2,4-heptadienal, (E,E)-,formic acid, heptyl ester,1,3-hexadiene
TiO_2 cataltytically treated COFs	4,6-decadiene, trans-3-Nonen-2-one, cycloheptanol, 2-methylene, 2(3H)-furanone, dihydro-5-pentyl-, 2-nonenal, (E)-, octanoic acid, 9-oxa-bicyclo[3.3.1]nona-3,6-dien-2-one, trans-2-undecenoic acid, 2-undecanone, 6,10-dimethyl-, 2,4-nonadienal, (E,E)-, trans-undec-4-enal, dodecane, decanal, hexyl octyl ether, 2,4-nonadienal, (E,E)-, 3-hexadiene, 3-ethyl-2-methyl-, 1,4-cyclooctanedione, 13-tetradece-11-yn-1-ol, 3-isopropyl-5-methylhexan-2-one, 2(3H)-furanone, 5-butyldihydro-, 2-decenal, nonanoic acid, 6-undecanone, hexanoic acid, tridecyl ester, 2,4-decadienal, tridecanal, bicyclo[3.3.1]nonane-2,7-dione, 2,4-decadienal, 1-undecene, 8-methyl-, 2-undecenal, 9-hexadecenoic acid, 6-dodecanone, 2,4-dodecadiene, (E,Z)-, 2-methyl-7-oxabicyclo[2.2.1]heptane
TP nanocomposite catalytically treated COFs	2-Heptanone ketone, 4-pentenal, ethanol, 2-butoxy-, ethanedioic acid, 2-pentyl-,3,7-decadiene, 2,9-dimethyl-,cyclohexanol, 2,4-dimethyl-, octanal, 4-ethylcyclohexanol, formic acid, heptyl ester

Thermal durability

Figure 9 shows the evolution of CO_2 production and VOCs removal by continuously feeding the THC concentration of 100-120 ppm of COFs through the TP photocatalytic oxidation. The VOCs concentration of the treated COFs was less than 15 ppm, and the CO_2 production was 55 ppm. The removal efficiency of VOCs was up to 80 %, and the mineralization efficiency, calculated using the mass ratio of CO_2 produced to initial THC concentration, was 46 %.

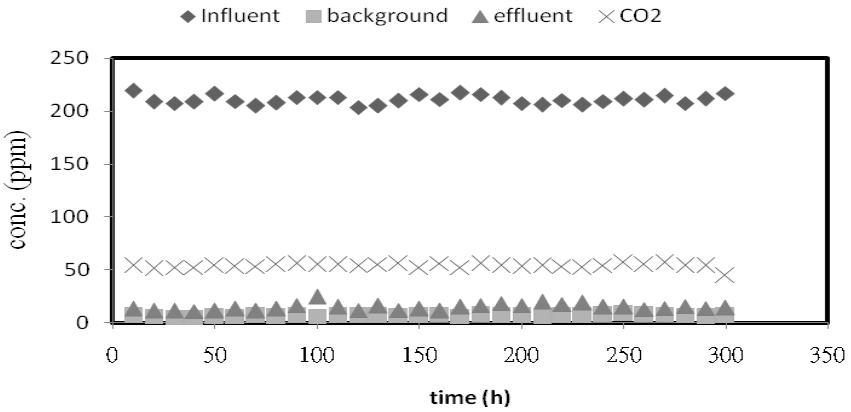

Fig-9: The CO_2 conversion and VOCs removal through TP photodegradation at 25^0C

The aforementioned result is unchanged until the reaction temperature is up to 125°C, and decreases in 125–250°C, and finally reduced to zero over 250 ^{0}C (Figure 10). This can be attributed to the thermal activated barrier. In PANI-metal oxide composites, the bonding between metal ion and nitrogen is not very strong and thermal activation energy due to a rise in temperature breaks the bond. Therefore, as temperature increases, the free charge carriers related with metal ion and the thermal vibrations of the sample contribute to increase the electrical resistance of the sample [36]. The temperature over critical value leads to the occurrence of the thermal degradation of skeletal PANI chain structure [37]. The results indicate that the developed TP photocatalyst revealed a comparable VOCs removal efficiency to certain frequently used techniques for COFs treatment such as biofiltration, condensation, wet scrubbing, and catalytic oxidation.

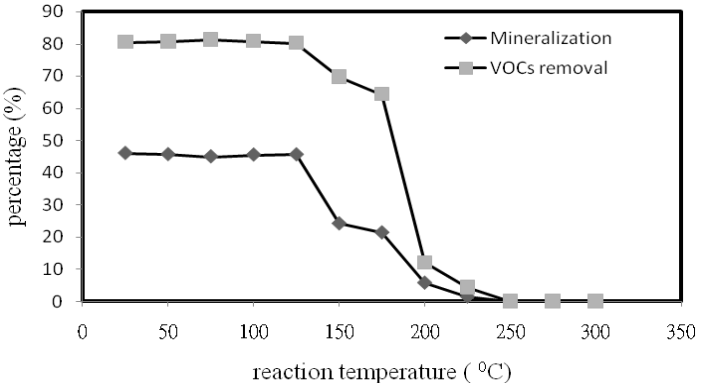

Fig-10: Temperature dependence of the CO_2 conversion and THC removal through TP photodegradation

CONCLUSIONS

In summary, a double–surfactant-assisted polymerization process was used to effectively synthesize a TP nanocomposite. The TP nanocomposite comprising a uniform nanoscale porous PANI shell coated onto the TiO_2 nanoparticles strongly absorbed light in the visible region of the solar spectrum. At an optimized AT ratio of 2.5, the TP nanocomposite exhibited higher photocatalytic activity toward COFs than did pure TiO_2. A thermal stability study revealed that the TP nanocomposite demonstrated a VOCs removal efficiency of 80% and mineralization efficiency of 46%, which were stable until the reaction temperature reached 125°C. This VOCs removal efficiency is comparable to those of traditional VOCs treatment technologies.

ACKNOWLEDGMENTS

The authors thank the National Central University, Taiwan, for its financial and technical support.

Conflict of Interest

All interests from the paper and the study belong only to the National Central University, Taiwan.

REFERENCES

[1] Lee, T., Gany, F. 2013. Cooking oil fumes and lung cancer: A review of the literature in the context of the U.S. population. Journal of Immigrant and Minority Health, 15(3), pp. 646–652.

[2] Maio, J. Y., Zeng, L. Y., Guo, X. F. 2005. Restaurant emissions removal by a biofilter with immobilized bacteria. Journal of Zhejiang University Science B, 6, pp. 433–437.

[3] Cheng, H. H., Hsieh, C. C. 2010. Integration of chemical scrubber with sodium hypochlorite and surfactant for removal of hydrocarbons in cooking oil fume. Journal of Hazardous Materials, 182, pp. 39–44.

[4] Wang, J. L., Zhong, J. B., Gong, M. C., Liu, Z. M., Ming, Z., Chen, Y. Q. 2007. Remove cooking fume using catalytic combustion over Pt/La-Al2O3. Journal of Environmental Sciences,19(6), pp. 644–646.

[5] Lin, B., & Liaw, S. L. 2015. Simultaneous removal of volatile organic compounds from cooking oil fumes by using gas-phase ozonation over Fe(OH)3 nanoparticles. Journal of Environmental Chemical Engineering, 3(3), pp. 1530–1538.

[6] Liu, Z. Q., Jiang, F. Y., Liu, R. C. 2012. Study on the preparation of nano TiO_2 powder and its properties. Applied Mechanics and Materials, 178-181, pp. 578–581.

[7] Nilsing, M., Persson, P. L. U., Lunell, S., Ojamaee, L. 2007. Dye-sensitization of the TiO_2 rutile (110) surface by perylene dyes: Quantum-chemical periodic B3LYP computation. Journal of Physical Chemistry C, 111(32), pp. 12116–12123.

[8] Kathirvel, S., Chen, H. S., Su, Wang, H. H., Li, C. Y., Wen-Ren L. 2013. Preparation of smooth surface TiO_2 photoanode for high energy conversion efficiency in dye-sensitized solar cells. Journal of Nanomaterials 2013, Article ID 367510, 8

[9] Polycarpos, F., Vrachnou, E., Gratzel, M., Nazeeruddin, M. K., Goff, A. H. L. 1993. Dye sensitization of TiO_2 surfaces studied by Raman spectroscopy Journal of the Electrochemical Society, 140(6).

[10] Bach, U., Lupo, D., Comte, P., Moser, J. E., Weissortel, F., Salbeck, J., Spreitzer, H., Gratzel, M. 1998. Solid-state dye-sensitized mesoporous TiO_2 solar cells with high photon-to-electron conversion efficiencies. Nature, 395, pp. 583–585.

[11] Wang, F., Min, S., Han, Y., Feng, L. 2010. Visible-lightinduced photocatalytic degradation of methylene blue with polyaniline-sensitized TiO_2 composite photocatalysts. Superlattices and Microstructures, 48, pp. 170–180.

[12] Wei, J., Zhang, Q., Liu, Y., Xiong, R., Pan, C., Shi, J. 2011. Synthesis and photocatalytic activity of polyaniline–TiO_2 composites with bionic nanopapilla structure. Journal of Nanoparticle Research, 13, pp. 3157–3165.

[13] Pawar, S. G., Patil, S. L., Chougule, M. A., Raut, B. T., Jundale, D. M., Patil, V. B. 2010. Polyaniline: TiO_2 nanocomposites: Synthesis and characterization. Archives of Applied Science Research, 2(2), pp. 194–201.

[14] Vivekanandan, J., Ponnusamy, V., Mahudeswaran1, A., Vijayanand, P. S. 2011. Synthesis, characterization and conductivity study of polyaniline prepared by chemical oxidative and electrochemical methods. Archives of Applied Science Research, 3(6), pp. 147–153.

[15] Bhadra, S., Khastgir, D., Singha, N. K., & Lee, J. H. (2009). Progress in preparation, processing and applications of polyaniline. Progress in Polymer Science, 34(8), pp. 783–810.

[16] Hayes, R., Ahmed, A., Edge, T., Zhang, H. 2014. Core–shell particles: Preparation, fundamentals and applications in high performance liquid chromatography. Journal of Chromatography A, 1357, pp. 36–52.

[17] Dubas, S. T., Kumlangdudsana, P., Potiyaraj, P. 2006. Layer-by-layer deposition of antimicrobial silver nanoparticles on textile fibers. Colloids and Surfaces A: Physicochemical and Engineering Aspects, 289(1–3), pp. 105–109.

[18] Misoon, O., & Seok, K. (2011). Effect of dodecyl benzene sulfonic acid on the preparation of polyaniline /activated carbon composites by in situ emulsion polymerization. Electrochimica Acta, 59(1), pp. 196–201.

[19] Fan, X., Lin, L., Messersmith, P. B. 2006. Surface-initiated polymerization from TiO_2 nanoparticle surfaces through a biomimetic initiator: A new route toward polymer–matrix nanocomposites. Composites Science and Technology, 66, pp. 1195–1201.

[20] Borodko, Y., Habas, S. E., Koebel, M., Yang, P., Frei, H., Somorjai, G. A. 2006. Probing the interaction of poly(vinylpyrrolidone) with platinum nanocrystals by UV−Raman and FTIR. The Journal of Physical Chemistry. B 110, pp. 23052–23059.

[21] Siriviriyanun, J. A., O'Rear, E. A., Yanumet, N. 2007. Modification of polyester fabric properties by surfactant-aided surface polymerization. Journal of Applied Polymer Science, 103(6), pp. 4059–4064.

[22] Samitsu, S., Zhang, R., Peng, X., Krishnan, M. R., Fujii, Y., & Ichinose, I. (2013). Flash freezing route to mesoporous polymer nanofibre networks. Nature Communications, 4, 2653.

[23] Zagorny, M., Bykov, I., Melnyk, A., Lobunets, T., Zhygotsky, A., Pozniy, A., Shirokov, A., Ragulya, A. 2014. Surface structure, spectroscopic and photocatalytic activity study of polyaniline/TiO_2 nanocomposites. Journal of Chemistry and Chemical Engineering, 8, pp. 118–127.

[24] Bull, I., Xue, W. M., Burk, P., Boorse, R. S., Jaglowski, W. M., Koermer, G. S., Moini, A., Patchett, J. A., Dettling, J. C., Caudle, M. T. 2009. Copper CHA zeolite catalysts. U.S. Patent 7601662.

[25] Grootveld, M., Silwood, C. J. L., Claxson, A., Serra, B. B., Viana, M. 2001. Health effects of oxidized heated oils. Journal of Foodservice, 13, pp. 41–55.

[26] Ramsay, J. D. F., Booth, B. O. 1982. Neutron scattering and adsorption isotherm studies of structure in oxide sols and gels. Studies in Surface Science and Catalysis, 10, pp. 211–225.

[27] Thamaphat, K., Limsuwan, P., Ngotawornchai, B. 2008. Phase characterization of TiO_2 powder by XRD and TEM. Kasetsart Journal : Natural Science, 42, pp. 357–361.

[28] Ba-Abbad, M., Kadhum, A. H., Mohamad, A., Takriff, M. S., Sopian, K. 2012. Synthesis and catalytic activity of TiO_2 nanoparticles for photochemical oxidation of concentrated chlorophenols under direct solar radiation. International Journal of Electrochemical Science, 7, pp. 4871–4888.

[29] Zhang, B., Du, Y., Zhang, P., Zhao, H., Kang, L., Han, X., Xu, P. 2013. Microwave absorption enhancement of Fe_3O_4/polyaniline core/shell hybrid microspheres with controlled shell thickness. Journal of Applied Polymer Science, 130(3), pp. 1909–1916.

[30] Lee, J. T. Y., Chow, K. L. 2011. SEM sample preparation for cells on 3D scaffolds by freeze-drying and HMDS. Scanning, 33, pp. 1–14.

[31] Hou, Q., Grijpma, D. W., Feijen, J. 2003. Preparation of interconnected highly porous polymeric structures by a replication and freeze drying process. Journal of Biomedical Materials Research Part B, 67B, pp. 732–740.

[32]Aranaz, I., Gutiérrez, M. C., Ferrer, M. L., del Monte, F. 2014. Preparation of chitosan nanocomposites with a macroporous structure by unidirectional freezing and subsequent freeze-drying. Marine Drugs, 12, pp. 5619–5642.

[33] Min, S., Wang, F., Han, Y. 2007. An investigation on synthesis and photocatalytic activity of polyaniline sensitized nanocrystalline TiO_2 composites. Journal of Material Science, 42, pp. 9966–9972.

[34] Li, X., Wang, D., Luo, Q., An, J., Wang, Y., Cheng, G. 2008. Surface modification of titanium dioxide nanoparticles by polyaniline via an in situ method. Journal of Chemical Technology and Biotechnology, 83, pp. 1558–1564.

[35] Sivachandiran, L., Thevenet, F., Gravejat, P., Rousseau, A. 2013. Isopropanol saturated TiO_2 surface regeneration by non-thermal plasma: Influence of air relative humidity. Chemical Engineering Journal, 214, pp. 17–26.

[36] Mothi, K. M., Soumya, G., Sugunan, S. 2014. Effect of calcination temperature on surface morphology and photocatalytic activity in TiO_2 thin films prepared by spin coating technique. Bulletin of Chemical Reaction Engineering & Catalysis, 9(3), pp. 175–181.

[37] Parveen, A., Roy, A. 2013. Effect of morphology on thermal stability of core-shell polyaniline/TiO_2 nanocomposites. Advanced Materials Letters, 4(9), pp. 696–701.

INTERNATIONAL JOURNAL OF PLANT, ANIMAL AND ENVIRONMENTAL SCIENCES

ISSN 2231-4490

International Journal of Plant, Animal and Environmental Sciences